2018

Hybrid Inductive Power Transfer and Wireless Antenna System for Biomedical Implanted Devices

Reem Shadid

Mohammad Haerinia
mohammad.haerinia@und.edu

Sayan Roy

Sima Noghanian
University of North Dakota, sima.noghanian@engr.und.edu

Progress In Electromagnetics Research C, Vol. 88, 77–88, 2018

Hybrid Inductive Power Transfer and Wireless Antenna System for Biomedical Implanted Devices

Reem Shadid[1], Mohammad Haerinia[1], Sayan Roy[2], and Sima Noghanian[1, *]

Abstract—In this paper, we present a hybrid system consisting of a novel microstrip antenna that can be designed to resonate at various frequencies within the ultra-high frequency (UHF) band (e.g., 415 MHz, 905 MHz, and 1300 MHz), combined with a pair of high frequency (HF) coils (13.56 MHz). The system is designed to be fabricated on an FR4 substrate layer, and it provides a compact solution for simultaneous wireless power transfer (WPT) and multi-band wireless communication, to be utilized in implanted medical devices. The external antenna/coil combination (EX) will be located outside the body on the skin layer. The EX has 79.6 mm-diameter. The implanted hybrid combination (IM) has 31.5 mm-diameter. The antenna is designed such that by varying the position of a shorting pin the resonance frequency can be changed among three frequencies; therefore, the same design can be used for various applications. The system was designed using numerical simulation tools, and then it was fabricated and measured. The design was optimized while the performance of the system was numerically simulated at various depths inside a layered body model. Furthermore, the insertion loss (S_{21}) and transmission efficiency (η) for both antenna and coil pairs at different depths were studied through simulation and measurements. The system provides a good solution for the combination of power transfer and multi-band data communication.

1. INTRODUCTION

Recently, WPT technologies have been widely adopted as a power source for implanted and wearable biomedical devices, since they provide convenience and portability. While the use of WPT is a nice addition to health-monitoring systems that have greatly affected t human healthcare [1, 2], they should be carefully designed and studied to make sure of the reliability of their performance. The communication link and WPT may require large size antennas and coils for the two systems. The system includes two parts: the EX part and IM one. An example of such systems is glucose monitoring systems such as [3]. In such a system, IM is a sensor that through the wireless communication channels sends the sensor signals of glucose level and blood pressure to EX equipment. These types of sensors fall under health-monitoring systems that are being developed for multiple purposes such as monitoring patients, fire-fighters, astronauts, and soldiers [4, 5].

WPT and communication both need bulky transmitters and receivers. Therefore, our major challenge is miniaturizing the communication and WPT systems. The unification and combination of the two systems provides the means of miniaturization of the overall system.

In proposing such systems, we consider: (1) a method that can be adopted for multiple frequencies, and (2) combining the WPT and communication links in a hybrid system to minimize the form-factor. Multiple frequency bands may be used to control multiple IM devices simultaneously. Also, each frequency band might be used for a different wireless link sending data, images, or control signals. The

Received 16 June 2018, Accepted 23 October 2018, Scheduled 7 November 2018

* Corresponding author: Sima Noghanian (sima.noghanian@engr.und.edu).

[1] School of Electrical Engineering and Computer Science, College of Engineering and Mines, University of North Dakota, USA. [2] Department of Electrical and Computer Engineering, College of Engineering, North Dakota State University, USA.

major limiting factors in these devices are the size of antennas and coils. Many techniques and methods have been proposed and used to minimize the size of microstrip antennas at a certain frequency. One common method to reduce antenna size is the use of high permittivity substrates [6]. However, this method has a negative influence on impedance bandwidth. Other methods have been used such as slot loading of the patch, e.g., U-shaped or H-shaped slots, to enhance the effective electrical length of the current path and to minimize the antenna size [7, 8]. In [9], authors applied a shorting pin technique to design a compact microstrip antenna working in free-space. In [10] authors presented a dual-band design for WPT consisting of IM and EX part. However, they used a complicated design for IM part, using multiple capacitors.

In this paper, we propose a compact hybrid design consisting of a pair of optimized inductive coils to transfer power wirelessly, and a novel antenna in a G-shaped design for data communication. A shorting pin is used to reduce the antenna size, whereas the location of the shorting pin inside the antenna determines its resonance frequency (f_{oEX} and f_{oIM}, for EX and IM, respectively). The coil size was optimized for the best efficiency and size, using a method that will be explained in Section 4.

This paper is organized as follows. Section 2 provides the information about the system and the layered body model. The details of antenna design are presented in Section 3. The design of coils is presented in Section 4. Section 5 gives details of calculation of efficiency and the specific absorption rate (SAR). Details of fabrication and measurements are provided in Section 6. A summary and conclusions are provided in Section 7.

2. SYSTEM MODEL

For this design we consider that the EX antenna/coil combination is placed directly at the outer surface of the skin, and the IM antenna/coil combination is embedded inside the muscle tissue. In the simulation model, layers of fat and skin cover the muscle layer. We start the design by assuming that IM combination is located at the depth (h) of 15 mm from the EX combination. The layered body model, consisting of three tissue layers, the skin layer (3 mm), the fat layer (7 mm), and the muscle layer (125 mm) are shown in Figure 1. All three layers have 212 mm $\times$ 212 mm surface area. It is assumed that IM and EX are covered by a layer of silicone with a thickness of 100 µm. Figure 1 also shows the combination of the EX and IM. The details of EX and IM dimensions are presented in Sections 3 and 4.

The electromagnetic properties of each tissue layer at each frequency were obtained from the Institute of Applied Physics (IFAC) database [11] and are summarized in Table 1. The substrates for IM ad EX are assumed to be FR4 with $\varepsilon_r = 4.4$ and $\tan\delta = 0.02$. The substrate thickness for EX

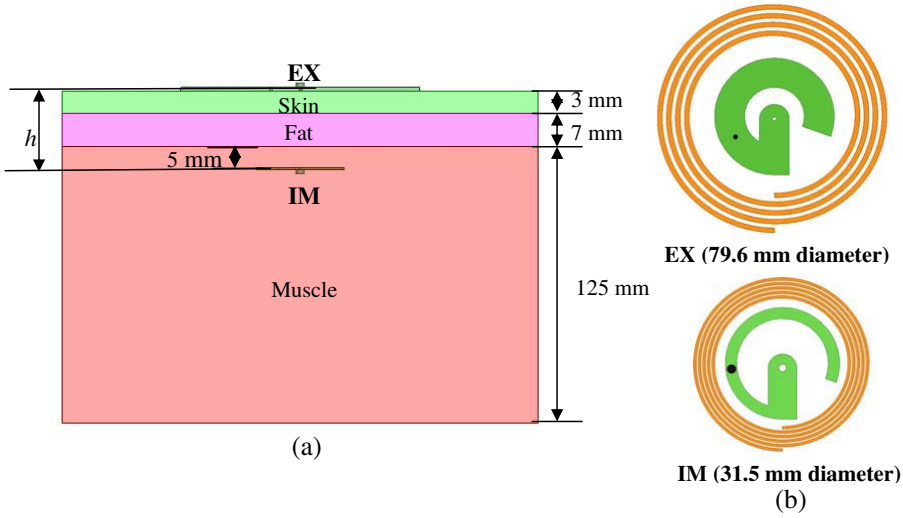

Figure 1. (a) Layered body model and (b) antenna and coil hybrid design of the EX and IM antenna/coil combinations. Reproduced courtesy of The Electromagnetics Academy.

Table 1. Tissues' electromagnetic properties at different frequencies.

f (MHz)	Tissue	ε_r	σ	tanδ
13.56	Muscle	138.44	0.63	6.01
	Fat	11.83	0.03	3.4
	Skin	285.25	0.24	1.10
415	Muscle	57.00	0.80	0.61
	Fat	5.57	0.04	0.32
	Skin	46.50	0.69	0.65
905	Muscle	55.00	0.94	0.34
	Fat	5.46	0.05	0.18
	Skin	41.40	0.87	0.42
1300	Muscle	54.20	1.09	0.28
	Fat	5.40	0.06	0.15
	Skin	39.90	1.00	0.34

is 1.52 mm, while for IM thickness is 0.8 mm. The copper thickness is assumed to be 35.56 µm for both IM and EX.

3. ANTENNA DESIGN

The EX and IM microstrip antennas have a G-shape profile. This design provides simplicity and low fabrication cost as well as small antenna size. The patch antenna is fed by a probe, and the resonance frequency can be adjusted by moving the shorting pin. The antenna geometry is shown in Figure 2, where R_{out} is the outer radius, R_{in} the inner radius, R_e the middle edge radius, g the distance between the center of the antenna circle and the feeding probe, R_g the ground circular slot radius, D_s the diameter of the shorting pin, D_f the diameter of the feeding probe, and Φ the arc angle.

The designed parameters values for EX and IM antennas are presented in Table 2. The antennas were simulated using ANSYS HFSS software [12]. A shorting pin is used to reduce the antenna size.

The number and position of shorting pins affect the resonance frequency (f_o) of the microstrip patch antenna. In free-space [13], the resonance frequency, f_o, can be obtained from Eq. (1).

$$f_o = \frac{c}{2(R_{out} + R_{in})\Phi_{radians}\sqrt{\varepsilon_{eff}}} \tag{1}$$

where c is the speed of light, Φ the arc angle in radians, and ε_{eff} the effective dielectric constant and

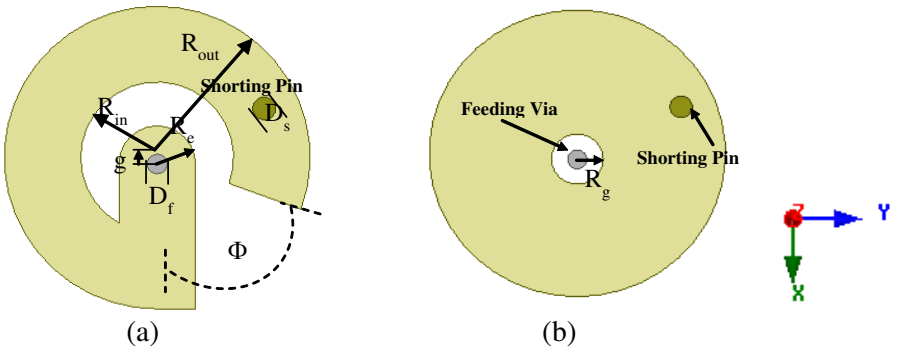

Figure 2. Antennas' geometry of (a) top radiating patch layer, and (b) ground plane.

Table 2. Parameters of antennas' geometry.

Parameter	EX antenna	IM antenna
R_{out} (mm)	20.0	10
R_{in} (mm)	10.0	8.0
R_e (mm)	5.0	2.5
g (mm)	0.8	0.8
R_g (mm)	2.0	2.0
D_s (mm)	1.6	1.6
D_f (mm)	1.3	1.3
Φ (degree)	70.0	70.0

calculated using Eq. (2).

$$\varepsilon_{eff} \approx \frac{\varepsilon_r + 1}{2} \tag{2}$$

Frequency domain solver in ANSYS HFSS was used to perform parametric study and find the best location of the shorting pin. Using parametric optimization, two variables of x and y coordinates of the shorting pin were varied to achieve the antenna resonance frequencies at three UHF frequencies (415 MHz, 905 MHz, and 1300 MHz). We used Eq. (1) to determine the initial values of R_{out} and R_{in} in free-space as a starting point for the optimization process. Then the optimization procedures consider the existence of body layers and optimize the final size parameters. The pin positions, in reference to the antenna center, are summarized in Table 3. These antenna designs do not require any matching circuit, since the antenna is matched to 50 Ω at the resonance frequency.

Table 3. Shorting pin locations for EX and IM antennas assuming antenna center is at $(0, 0)$, all dimensions are given in mm.

Antenna	*Location*	415 MHz	905 MHz	1300 MHz
EX	x	-6.50	6.75	11.00
	y	14.00	-13.00	-5.50
IM	x	2.25	1.08	6.72
	y	8.70	-8.88	-5.95

4. COILS DESIGN

Coil geometry and design is shown in Figure 3. The most important consideration in design of a WPT system is to maximize the efficiency of the power transfer. Optimization was done in two stages. The first stage was based on the design presented in [14], and the optimum values of the inner diameter (d_{in}) for EX and IM coils were chosen, considering the optimum distance between the coil and the antenna required for the minimum coupling. In the second stage of optimization, the rest of the coil geometrical parameters including the coil trace (w), coil space (s), and the number of turns (n) were optimized using the parametric optimization tool in ANSYS Maxwell [12]. The values were selected based on the maximum coupling coefficient (k) that could be achieved between the EX and IM coils taking into consideration the maximum outer diameter (d_{out}) that is needed for the coils. The results are summarized in Table 4.

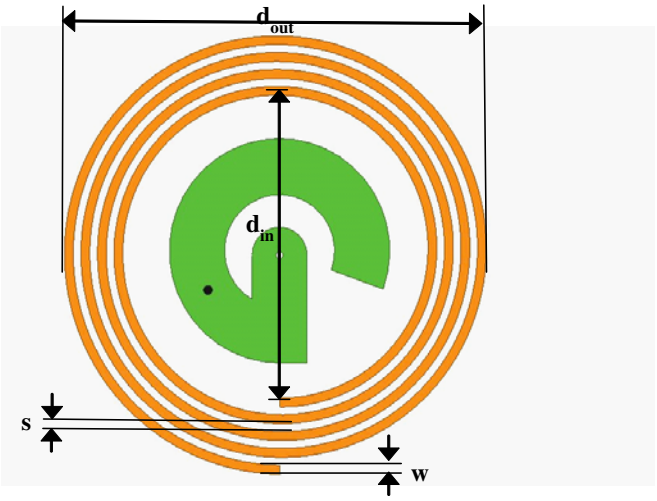

Figure 3. Geometrical parameters of a circular planar spiral coil. Reproduced courtesy of The Electromagnetics Academy.

Table 4. Parameters of EX and IM coils.

Parameter	EX coil	IM coil
d_{out} (mm)	79.6	31.5
d_{in} (mm)	54.0	23.0
s (μm)	1400.0	300.0
w (μm)	1600.0	500.0
n	4.0	5.0

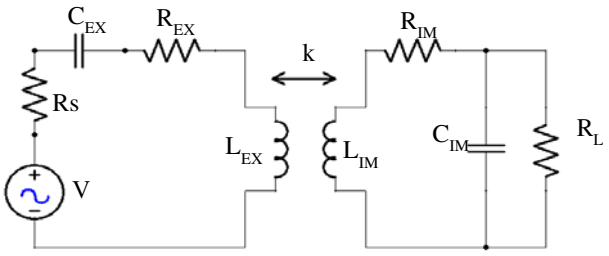

Figure 4. A simplified circuit diagram for the inductive link with matching capacitors. Reproduced courtesy of The Electromagnetics Academy.

The coils were designed to transfer power at $f_{coil} =$ 13.56 MHz. The simplified circuit diagram of the power flow through coils inductive link, as well as the lumped capacitors elements, added for matching, are shown in Figure 4 [10, 15]. L_{EX}, R_{EX}, C_{EX} represent the inductance, resistance and the matching capacitance of the EX coil, respectively. L_{IM} , R_{IM} , C_{IM} represent the inductance, resistance and the matching capacitance of the IM coil, respectively. R_s is the source resistance, R_L the load resistance, and k the coupling coefficient between the EX and IM coils. The values of C_{EX} and C_{IM} are chosen to satisfy Eq. (3). This circuit was simulated by ANSYS Simplorer. Table 5 summarizes the circuit element values.

$$f_{coil} = \frac{1}{2\pi\sqrt{L_{EX}C_{EX}}} = \frac{1}{2\pi\sqrt{L_{IM}C_{IM}}} \tag{3}$$

Table 5. Circuit element parameters for the inductive link, referring to Figure 4.

Parameter	EX coil
L_{EX} (µH)	1.783
R_{EX} (mΩ)	357.27
C_{EX} (pF)	77.26
L_{IM} (µH)	1.204
R_{IM} (mΩ)	567.31
C_{IM} (pF)	114.42
R_L (Ω)	50.00
R_S (Ω)	50.00
k at $h = 15$ mm	0.113

5. EFFICIENCY AND SAR CALCULATIONS

To study the performance of the system in implanted devices, the effect of the implanting depth on the stability of resonance frequencies of antennas, f_{oEX} and f_{oIM}, at each resonance frequency of interest (415 MHz, 905 MHz, and 1300 MHz) was studied. Furthermore, the transmission efficiency (η) at different distances was calculated for either coil or the antenna pair, using Eq. (4).

$$\eta = |S_{11}|^2 \times 100\% \tag{4}$$

where S_{21} is the transmission coefficient, and it is referring to a ratio of signal exiting at an output port to a signal incident at an input port. For the pair of antennas, ANSYS HFSS simulation program was used to extract S_{21} directly, whereas for the coil pair this value was extracted by importing the coil design into ANSYS Maxwell and integrating it with the circuit in ANSYS Simplorer, as shown in Figure 4.

For any implanted device it is important to consider the safe levels of power absorbed by the tissue. SAR analysis is used to measure the amount of electromagnetic energy absorbed by a lossy dielectric material. To calculate SAR for this system HFSS simulation was used. SAR was calculated using Eq. (5).

$$SAR = \frac{\sigma}{2\rho} E^2 \tag{5}$$

where σ is the conductivity of the tissue, ρ the mass density of the mass of tissue per unit volume, and E the electric field strength inside the tissue.

The time domain solver in HFSS was used to calculate the SAR. The system was tested at every proposed UHF frequency. The peak SAR values reach 0.43 W/kg, 0.58 W/kg, and 0.654 W/kg in 10 g of average mass at 415 MHz, 915 MHz, and 1300 MHz, respectively. These values are well below the regulatory limit of 2 W/kg averaged over 10 g of tissue based on ICNIRP regulation [16]. Figure 5 shows the cross-section of yz-plane for all frequency cases. The highest value of SAR occurs at 1300 MHz, and there is more penetration into the tissue layer for this frequency. The small dialog box shows the values for the color bar.

6. MEASUREMENT RESULTS

EX and IM coil/antenna combinations for each resonance frequency (different shorting pin locations) were fabricated on an FR-4 substrate, as shown in Figure 6. A muscle phantom based on the method described in [17] was fabricated. Figure 7 shows the measurements setup.

The simulated values of f_{oEX} and f_{oIM} when IM is located at different depths (h values ranging between 15 mm and 110 mm) are summarized in Table 6. It is notable that the resonance frequency of the antennas does not change more than 20 MHz while the implant depth (h) is changed. Therefore,

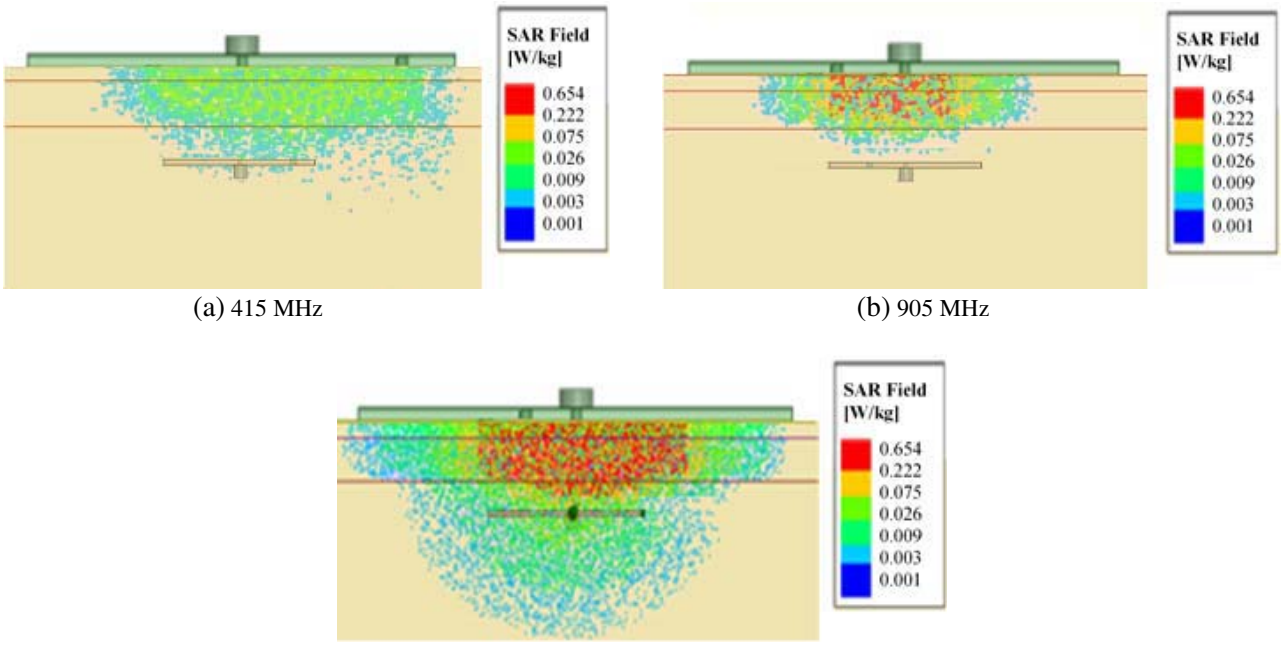

(a) 415 MHz (b) 905 MHz

(c) 1300 MHz

Figure 5. Simulated antenna SAR analysis at (a) 415 MHz, (b) 905 MHz, and (c) 1300 MHz. Reproduced courtesy of The Electromagnetics Academy.

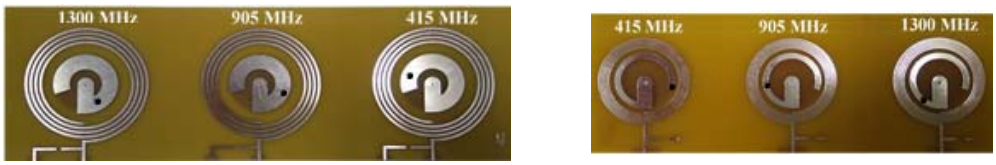

(a) (b)

Figure 6. Fabricated combinations of coil/antenna for (a) EX and, (b) IM. Reproduced courtesy of The Electromagnetics Academy.

Table 6. Resonance frequencies of antennas at different implanting depth. Reproduced courtesy of The Electromagnetics Academy.

h (mm)	415 (MHz)		905 (MHz)		1300 (MHz)	
	f_{oEX}	f_{oIM}	f_{oEX}	f_{oIM}	f_{oEX}	f_{oIM}
15	415	415	905	905	1300	1300
20	415	410	910	900	1295	1290
30	415	410	905	905	1300	1300
40	415	410	905	905	1300	1300
50	415	410	905	910	1300	1300
60	415	410	905	905	1300	1300
70	415	410	905	905	1300	1300
80	415	410	905	905	1300	1300
90	415	410	905	905	1300	1300
100	415	410	905	905	1300	1300
110	415	410	905	905	1295	1300

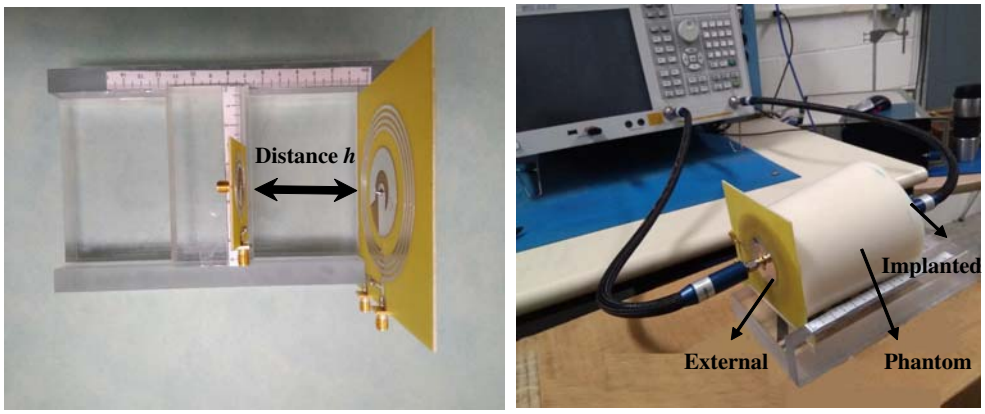

Figure 7. Measurement setup in (a) air and, (b) phantom. Reproduced courtesy of The Electromagnetics Academy.

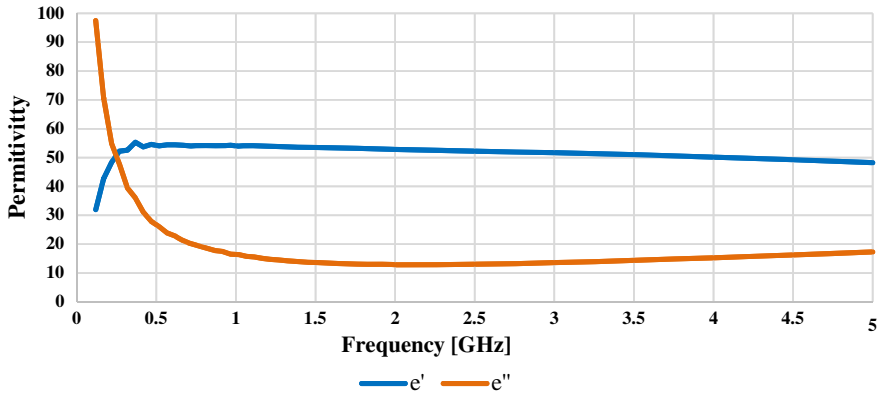

Figure 8. Measured permittivity value for the muscle phantom. Reproduced courtesy of The Electromagnetics Academy.

it is concluded that the three proposed G-shape antennas resonance frequencies are not affected by the implanting depth, and the distance between the EX and IM antennas. The performance of the antennas at all bands at $h = 15$ mm was studied experimentally.

To evaluate the system experimentally, a phantom was fabricated that represents muscle tissue. The phantom properties were measured by Keysight 85070E high performance dielectric probe. The S-parameters were measured by a Keysight E5071C Vector Network analyzer (VNA). Figure 8 shows the measured permittivity of the phantom. The minimum reflection coefficients were achieved by simulation for the EX and IM antennas, and S_{11} and S_{22} with -10 dB bandwidth are summarized in Table 7. The simulated as well as the measured S_{11}, S_{22} and, S_{21} at the same h are depicted in Figure 9. Please note that the maximum value of S_{21} occurs at the 905 MHz and 1300 MHz, whereas at 415 MHz it has lower transfer coefficient and efficiency.

Table 7. Antennas's parameters and bandwidth.

Description	415 (MHz)	905 (MHz)	1300 (MHz)
S_{11} (dB)	-13.81	-45.25	-15.23
-10 dB EX Bandwidth (GHz)	0.38–0.45	0.820–1.03	1.192–1.45
S_{22} (dB)	-15.88	-24.99	-37.94
-10 dB IM Bandwidth (GHz)	0.36–0.48	0.79–1.04	1.16–1.45

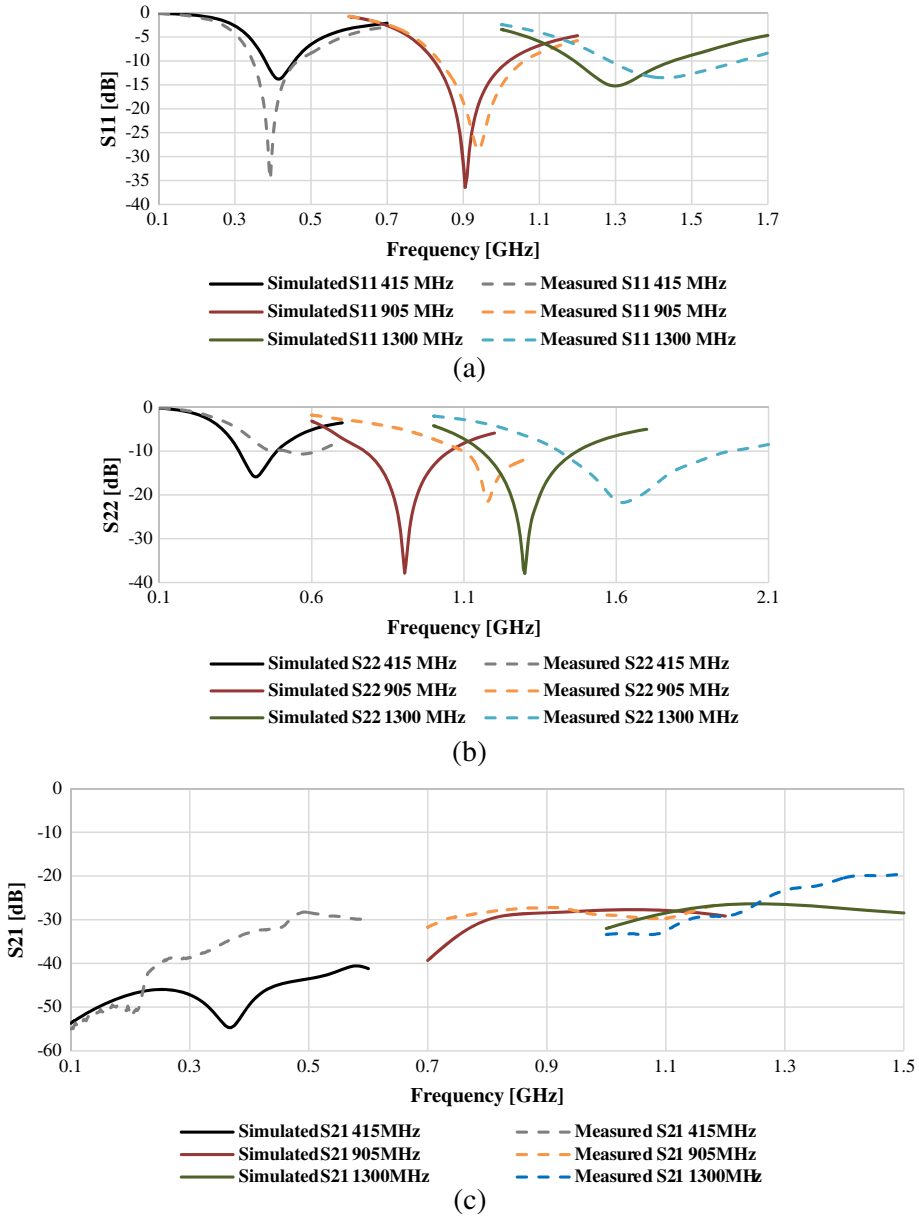

Figure 9. Simulated and measured S parameters of antennas versus frequency, (a) S_{11}, (b) S_{22} and (c) S_{21}. Reproduced courtesy of The Electromagnetics Academy.

The effect of implanting depth on S_{21} and η of EX and IM was studied. The simulated results for all S_{21} are plotted in Figure 10. We noticed that the behaviors of 905 MHz and 1300 MHz antennas were approximately the same. The comparison of measured and simulated S_{21} for each antenna and coil pair is shown in Figure 11. The results show very good agreement with simulated antenna especially for h less than 70 mm and for 905 MHz. The difference for larger h might be due to reflections and refractions from the sharp edges in the measurement structure.

Efficiency η is plotted in Figure 12. Coil provides inductive power transfer while the antennas, if used for power transfer, provide radiative power. The inductive link has much better η than the radiative one for distances less than 60 mm. At the implant depth of 60 mm η for both will be approximately the same. We noted that at $h = 10$ mm, the value of S_{21} is less than that of $h = 15$ mm. This may have happened due to antennas being in the near-field of each other, or due to the reflections from the surface.

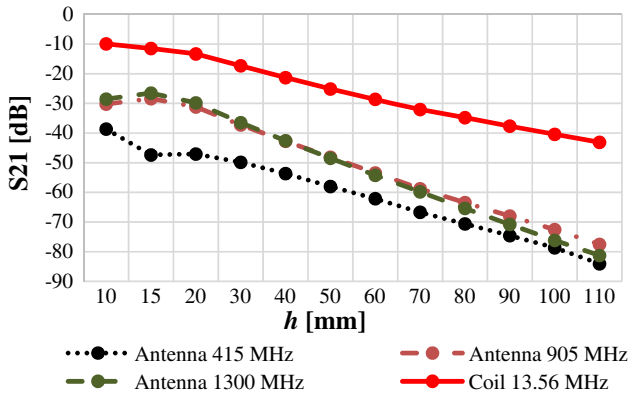

Figure 10. S_{21} versus h depth. Reproduced courtesy of The Electromagnetics Academy.

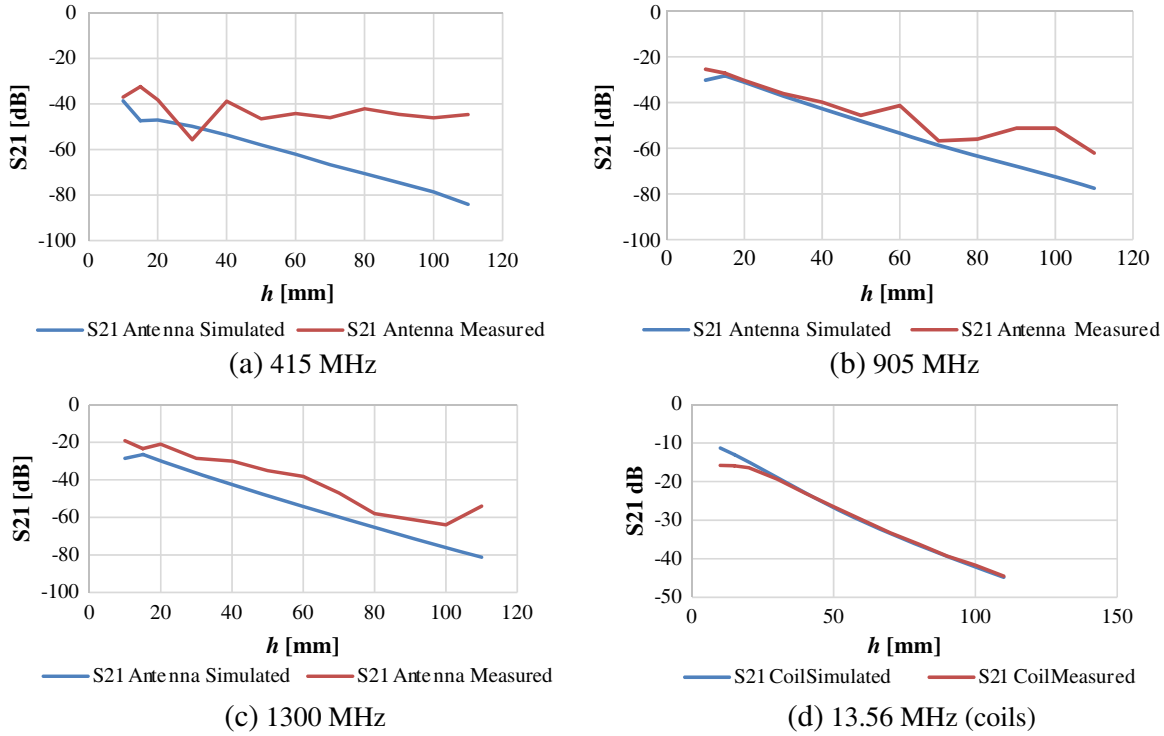

Figure 11. S_{21} versus h depth. Reproduced courtesy of The Electromagnetics Academy.

Power efficiency (η_P) was calculated using (6),

$$\eta_p = \frac{\mathrm{Re}(P_{out})}{\mathrm{Re}(P_{in})} \times 100\% \tag{6}$$

where $\mathrm{Re}(P_{out})$ is the real part of the output power, and $\mathrm{Re}(P_{in})$ is the real part of the input power. Figure 13 shows the power efficiency versus the depth of implant (h) for the inductive link coil, and 72.26% at $h = 15$ mm was achieved. As the distance increases between the EX and IM combinations, the efficiency drops.

The coil impedance was also measured using the same VNA. This measurement showed the inductance of 1.82 µH and resistance of 366 mΩ for the EX coil. On the other hand, the inductance value of the IM coil is 1.043 µH, and its resistance is 611 mΩ. These values agree well with the simulated one.

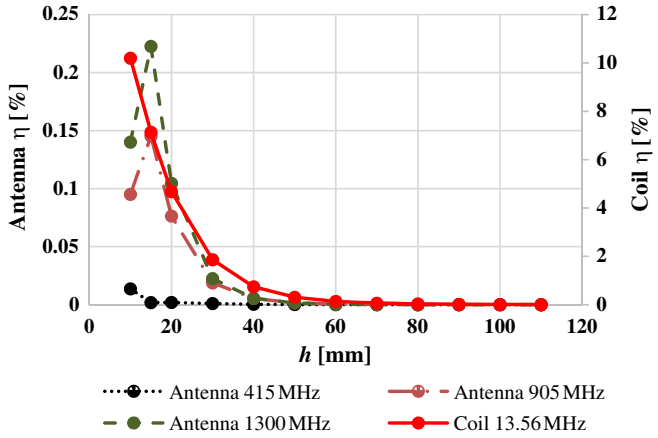

Figure 12. Efficiency of antenna and coil versus implanting depth. Reproduced courtesy of The Electromagnetics Academy.

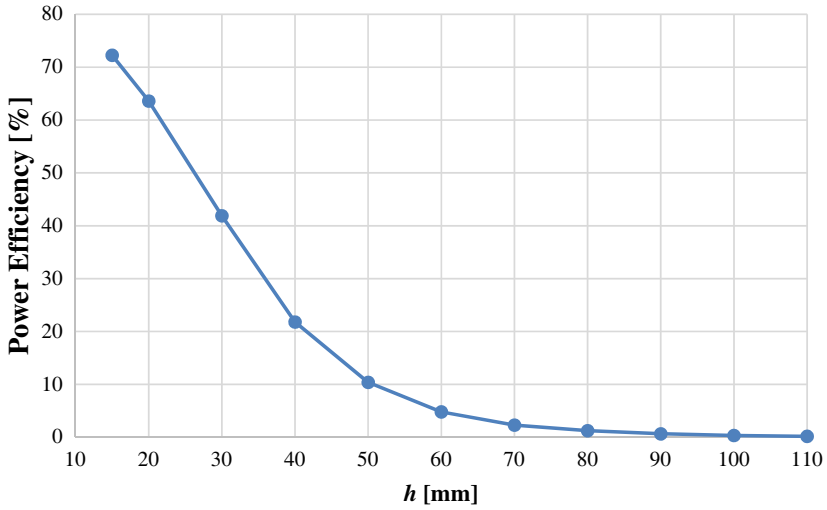

Figure 13. Power efficiency versus implanting depth for the inductive link coil. Reproduced courtesy of The Electromagnetics Academy.

7. CONCLUSION

In this paper we proposed and investigated the performance of a hybrid system that combines the G-shaped antennas (used for communication) and coils (used for WPT). The antennas could be adjusted to work at one of the three different frequencies (415 MHz, 905 MHz, and 1300 MHz) by changing the location of a shorting pin. The coils are designed to transfer power at 13.56 MHz. It was assumed that the implanted combination antenna and coil would be placed 15 mm from the external antenna/coil combination. A layered body model, consisting of three tissue layers, skin, fat, and muscle, was considered. The performance of this hybrid system was studied by calculating the efficiency. Also the safety levels were studied by calculation of the SAR. The system provides a good solution for wireless link for signal combination and WPT, in a compact design.

ACKNOWLEDGMENT

This work was supported by North Dakota Department of Commerce through a Venture Phase I grant and the Applied Science University of Jordan. The author would like to acknowledge the help of Mr. Milad Mirzaee, Mr. Robert Brunnemer and Ms. Ala Alemaryeen.

REFERENCES

1. Clark, G., *Cochlear Implants: Fundamentals and Applications*, 2003.
2. Weiland, J. D. and M. S. Humayun, "Retinal prosthesis," *IEEE Trans. Biomed. Eng.*, Vol. 61, No. 5, 1412–1424, 2014.
3. Ahmadi, M. M. and G. A. Jullien, "A wireless-implantable microsystem for continuous blood glucose monitoring," *IEEE Trans. Biomed. Circuits Syst.*, Vol. 3, No. 3, 169–180, 2009.
4. Xie, L., Y. Shi, Y. T. Hou, and A. Lou, "Wireless power transfer and applications to sensor networks," *IEEE Wirel. Commun.*, Vol. 20, No. 4, 140–145, 2013.
5. Xie, L., Y. Shi, Y. T. Hou, and H. D. Sherali, "Making sensor networks immortal: An energy-renewal approach with wireless power transfer," *IEEE/ACM Trans. Netw.*, 1350–1358, 2012.
6. Chaloupka, H., N. Klein, M. Peiniger, H. Piel, A. Pischke, and G. Splitt, "Miniaturized high-temperature superconductor microstrip patch antenna," *IEEE Trans. Microw. Theory Tech.*, Vol. 39, No. 9, 1513–1521, 1991.
7. Chair, R., K. M. Luk, and K. F. Lee, "Small dual patch antenna," *Electron. Lett.*, Vol. 35, No. 10, 762, 1999.
8. Chiu, C. Y., C. H. Chan, and K. M. Luk, "Small dual-band antenna with folded-patch technique," *IEEE Antennas Wirel. Propag. Lett.*, Vol. 3, No. 1, 108–110, 2004.
9. Yu, X., G. Li, and Z. Wang, "Design of compact 2.45 GHz microstrip antenna," *2005 IEEE International Symposium on Microwave, Antenna, Propagation and EMC Technologies for Wireless Communications*, Vol. 1, 153–156, 2005.
10. Sharma, A., E. Kampianakis, and M. S. Reynolds, "A dual-band HF and UHF antenna system for implanted neural recording and stimulation devices," *IEEE Antennas Wirel. Propag. Lett.*, Vol. 16, 493–496, 2017.
11. "Institute of applied physics (IFAC)," [Online], Available: http://niremf.ifac.cnr.it/tissprop/htmlclie/htmlclie.php.
12. Ansys, Inc., [Online], Available: www.ansoft.com.
13. Thakare, V. V., P. Singhal, and K. Das, "Calculation of Microstrip antenna bandwidth using Artificial Neural Network," *2008 IEEE Int. RF Microw. Conf.*, 404–406, 2008.
14. Shadid, R. and S. Noghanian, "Hybrid power transfer and wireless antenna system design for biomedical implanted devices," *ACES Conference in Denver*, 2018.
15. Shadid, R. and S. Noghanian, "A literature survey on wireless power transfer for biomedical devices," *Int. J. Antennas Propag.*, Vol. 2018, No. 5, 1–11, 2018.
16. International Commission on Non-Ionizing Radiation Protection, "Guidelines for limiting exposure to time-varying electric, magnetic, and electromagnetic fields (up to 300 GHz)," *Health Phys.*, Vol. 75, No. 5, 535, 1998.
17. Yilmaz, T., R. Foster, and Y. Hao, "Broadband tissue mimicking phantoms and a patch resonator for evaluating noninvasive monitoring of blood glucose levels," *IEEE Trans. Antennas Propag.*, Vol. 62, No. 6, 3064–3075, 2014.